Journal of Civil and Hydraulic Engineering
https://www.acadlore.com/journals/JCHE

Mechanisms of Cracking and Stress Control During the Construction Phase of Concrete Face Rockfill Dams in Cold Regions

Junbang Duan[1], Qiujing Zhou[2,3*], Wendong Zhao[1], Jinghong Zhao[4], Jianbo Li[1], Yanna Li[2,3]

[1] Country Qinghai Yellow River Upstream Hydropower Development Corporation Limited Engineering Construction Branch, 810006 Xining, China
[2] Country China Institute of Water Resources and Hydropower Research, 100038 Beijing, China
[3] State Key Laboratory of Watershed Water Cycle Simulation and Regulation, 100038 Beijing, China
[4] Power China Chengdu Engineering Corporation Limited School of Civil Engineering, 610072 Chengdu, China

* Correspondence: Qiujing Zhou (zhouqj@iwhr.com)

Received: 01-29-2024 **Revised:** 03-18-2024 **Accepted:** 03-25-2024

Citation: J. B. Duan, Q. J. Zhou, W. D. Zhao, J. H. Zhao, J. B. Li, and Y. N. Li, "Mechanisms of cracking and stress control during the construction phase of concrete face rockfill dams in cold regions," *J. Civ. Hydraul. Eng.*, vol. 2, no. 2, pp. 87–99, 2024. https://doi.org/10.56578/jche020202.

Abstract: The construction phase of concrete face rockfill dams is often marred by prominent panel cracking issues, with a lack of reliable foundations for anti-cracking design. To control tensile stresses and enhance crack resistance during construction, this study focuses on the primary factors influencing concrete panel stress in cold regions and the standards for crack resistance control. Through sensitivity analysis using simulation methods and incorporating case studies from typical projects, the mechanisms behind cracking were elucidated, and relevant recommendations were proposed. The research indicates that environmental temperatures in cold regions play a dominant role in load-related stresses, with daily temperature variations and cold waves acting as inducing factors. The impact of drying shrinkage is minimal under current conditions of adequate water curing, and the effect of panel deflection deformation is small. Regarding constraints, the influence of the bedding constraint is significant, whereas reinforcement measures have a minimal effect. Among performance parameters, casting temperature has a pronounced impact, as do autogenous volume changes and the coefficient of thermal expansion, while the influence of the adiabatic temperature rise varies insignificantly within a certain range. This study holds significant importance for the prevention of cracking in concrete face rockfill dam panels.

Keywords: Rockfill dam; Panel; Stress; Cracking; Crack resistance safety

1 Introduction

The concrete panel, as the main seepage control structure of the concrete face rockfill dam, its integrity and durability are crucial. Cracking prevention of the panel is an important issue that needs attention during design and construction. In the actual construction process of concrete face rockfill dams, panel cracking is very common [1, 2], especially during the construction phase [3–5]. For instance, Lv and Li [1] noted that among 13 surveyed high rockfill dams with panel cracking, 10 exhibited cracks during the construction phase. Marques Filho and De Pinto [6] analysed leakage and face crack incidents in some CFRD dams during construction and under reservoir loading.The fundamental cause of concrete panel cracking is that the dynamic forces causing cracking exceed the concrete's resistance to cracking. To reduce or avoid panel cracking, it is necessary to either reduce the dynamic forces causing cracking or to enhance the resistance to cracking, and extensive research has been conducted on both aspects.

Researchers like Yuan et al. [7], Li [8], and Zhao et al. [9] studied the impact of environmental temperature, humidity, and insulation and moisture retention measures on stress, proposing measures to reduce temperature stress and drying shrinkage stress; Chen et al. [10], Li [8], and Zhao et al. [11] researched the effects of performance parameters such as concrete casting temperature, adiabatic temperature rise, and thermal expansion coefficient on stress, clarifying the degree of influence of performance parameters on stress; Xie et al. [12] used simulation methods to analyze some factors affecting the spatiotemporal distribution characteristics of panel stress, revealing the distribution and variation patterns of stress, and proposing crack prevention measures; Zhang et al. [13] conducted

calculations of panel temperature stress due to solar radiation heat, considering the temperature stress caused by summer solar radiation as one of the important reasons for panel compression damage. These studies share a common understanding that changes in temperature and humidity, as well as temperature and humidity control measures, are the main factors affecting panel stress, especially during the construction period, where improper control can lead to cracking. Additionally, the high density of panel reinforcement and the interaction between steel and concrete deformation can affect concrete panel stress [14]. Rockfill dam deformation and panel disbonding are also significant factors, with researchers like Yang et al. [15], Liu et al. [16], Li et al. [17], and Jiang et al. [18] studying the impact of rockfill deformation and panel disbonding on panel stress. However, factors such as deformation and disbonding mainly occur during the operational phase, with their magnitude and impact generally not significant during the construction phase. Special loads such as earthquakes can also affect stress, with Kong et al. [19], Saberi et al. [20], and others conducting in-depth and systematic studies on the evolution of panel cracking under earthquake conditions.

In terms of enhancing panel crack resistance, work has been conducted around structures and materials. For example, Zhou et al. [21] proposed a composite structure of concrete gravity dams and rockfill dams, adding concrete dams (walls) at the dam heel, which shortened the length of the concrete panel. Based on the Daxia Gorge project, the results show that panel stress is within a reasonable range of the project; Zhao et al. [11] studied the thermal expansion coefficient of carbon nanotube-reinforced rockfill dam panel concrete in the early age, providing a reference for improving the thermal expansion coefficient of panel concrete.

Actual projects in cold regions as shown in Table 1. indicate that due to harsh climatic conditions, the difficulty of preventing panel cracking in rockfill dams is greater, with serious cracking issues during the construction phase. Inspections have shown that before impounding water at the Gongboxia Hydropower Station, 594 horizontal cracks appeared on the panel, and after water storage, vertical and horizontal cracks appeared in the water level fluctuation zone. Within 2 weeks after the completion of casting at the Jishixia Hydropower Station, 53 cracks were found, mainly horizontal cracks, distributed in the middle third of the panel. After the construction of the Nazixia Hydropower Station was completed, a total of 383 cracks were found. These three projects are located in the northwest of China, with a cold climate, and cracking mainly occurred in the early stage after construction completion, with temperature being the main influencing factor [22, 23]; after the dam was impounded, regular cracking occurred above the water surface of the Gongboxia reservoir, not obvious underwater, with temperature and drying shrinkage playing a major role; bottom surface constraints and erected reinforcement constraints could also have a certain impact.

Table 1. Main parameters of typical projects in cold regions

Project	Height (m)	Length of Crest	Average Temp (°C)	Pouring Time	Concrete	Pouring Method
Gongboxia	121.5	408	8.5	May-August	C25W12F200	Continuous
Jishixia	103	324	8.7	March-May	C25W12F200	Continuous
Nazixia	132.2	429	0.48	March-June	C30W12F300	Two phases

The panel, as a type of hydraulic concrete structure for dams, should undergo concrete crack resistance or crack limitation calculations according to relevant standards [24]. However, the current design standards for concrete face rockfill dams only specify the segmentation and thickness of panels and do not cover panel stress calculation and crack resistance safety requirements [25]. This lack of guidelines leads to a foundationless crack resistance safety analysis in actual engineering design and construction. This paper, taking the Yangqu panel rockfill dam as an example and considering loads, constraints, and performance parameters, employs the finite element simulation analysis method to study the sensitivity of the main factors affecting panel stress during the construction phase in cold regions. It aims to clarify the stress evolution pattern and crack resistance capability, providing references for crack prevention design and construction of the panel.

2 Computational Analysis Method and Crack Resistance Safety Standard

2.1 Computational Analysis Method

The stress analysis of the panel during construction involves temperature, humidity, rockfill dam deformation, reinforcement insertion, and bottom surface constraints, with related analysis theories and methods being relatively mature [26]. This section briefly introduces the simulation methods for drying shrinkage, reinforcement insertion, and bottom surface constraints.

Concrete drying shrinkage, caused by changes in humidity, is based on humidity field calculations. As a porous medium, concrete's humidity distribution follows Fick's second law, with the differential control equation for the non-steady humidity field as follows:

$$\frac{\partial h}{\partial t} = \frac{\partial}{\partial x}\left[k_h(h)\frac{\partial h}{\partial x}\right] + \frac{\partial}{\partial y}\left[k_h(h)\frac{\partial h}{\partial y}\right] + \frac{\partial}{\partial z}\left[k_h(h)\frac{\partial h}{\partial z}\right] - \frac{\partial Q}{\partial t}$$

where, t is time, h is humidity, k_h is the material's humidity diffusion coefficient, and $\frac{\partial Q}{\partial t}$ is the rate of humidity consumption due to cement hydration, with Q being the relative humidity content.

This equation is nonlinear and can be iteratively solved under known initial humidity and boundary conditions. The humidity diffusion coefficient k_h, a key parameter describing concrete's humidity and humidity field characteristics, is determined by the following equation in this study:

$$k_h = k_1 \left\{ \alpha + \frac{1-\alpha}{1+\left[(1-h)/(1-h_c)\right]^n} \right\}$$

where, k_1 is the maximum value of k_h when the humidity $h = 1, \alpha = k_0/k_1, k_0$ is the minimum value of k_h when the humidity $h = 0$; n the curve fitting exponent, h_c is the humidity corresponding to half the maximum value of the humidity diffusion coefficient; here, $\alpha = 0.05, h_c = 0.80, n = 15, k_1 = \frac{k_{1,o}}{f_{ck}/f_{cko}}$.

The change in concrete panel humidity is related to strain change. Typically, when humidity changes between 0.6 and 1.0 , it is assumed that the shrinkage strain increment $\Delta\varepsilon_s$ is directly proportional to the humidity increment Δh, with the drying shrinkage coefficient α_s approximately taken as 1.5×10^{-3}.

In the calculations, panel reinforcement is simulated using rod elements, assuming that the reinforcement is consolidated with the concrete, meaning both share the same strain. The reinforcement area A_s, elastic modulus E_s, and yield strength Y_s are all considered.

The bottom surface of the panel is subject to constraints, treated as a face-to-face contact problem and simulated using no-thickness contact elements, which can resist compression but not tension. The interaction between the panel and the bedding can lead to closure, opening, and shearing deformations, influenced by the values of normal stiffness, tangential stiffness, and strength parameters. Normal and tangential stiffnesses λ_n and λ_s are taken as 20 and 2 times the final elastic modulus of concrete, respectively.

Calculations use the self-developed structural multifield simulation and nonlinear analysis software SAPTIS [27], which have been applied and verified in over a hundred dams such as Liu et al. [28], considering the panel concrete casting process, hydration heat process, hardening process, and environmental temperature change process, to simulate the panel construction phase process. The calculation steps are 0.25d per step for the first 3 days, 0.5d per step for days 4-6, 1d per step for days 7-12, and then 2d and 5d steps up to 30 days.

2.2 Crack Resistance Safety Standard

Preventing panel cracking is an important issue in design and construction, with a current lack of feasible safety standards for crack control analysis. Referring to the concrete dam crack resistance safety control [29], the design tensile stress is defined as:

$$\sigma_{dt} = a_1 a_2 a_3 a_4 \sigma_t$$

where, σ_t is the calculated tensile stress, a_1 is the construction importance coefficient, with values of $1.1, 1.0$, and 0.9 for Class I, II, and III buildings respectively; a_2 is the correction coefficient for analysis errors due to temperature, humidity, and adiabatic temperature rise, with values of 1.1-1.2 considering the panel's significant susceptibility to cold snaps, daily temperature differences, and shrinkage; a_3 is the post-deformation age coefficient, taken as 1.0 for early ages; a_4 is the correction coefficient for construction quality, rockfill body deformation, etc., with values between 0.8-1.1, where a value greater than 1.0 is used when actual rockfill body deformation is large.

The usable tensile strength is defined as:

$$f_t = b_1 b_2 \, \mathrm{b}_3 \mathrm{R}_t$$

where, b_1 is the specimen size effect coefficient, where the panel concrete uses $100\ \mathrm{mm} \times 100\ \mathrm{mm}$ specimens to measure the ultimate tensile value and axial tensile strength, which is comparable to the panel thickness size, but there is a significant difference in length and width, thus this coefficient is taken as 0.80-1.0; b_2 is the time effect coefficient, the longer the load-bearing time, the smaller this value, taken as 0.7-0.9; b_3 is the post-age strength coefficient, mainly considering early-age crack resistance safety, taken as 1.0 .

From: $\sigma_{dt} \leq f_t$, the crack resistance safety factor K can be derived as:

$$K = \frac{a_1 \mathrm{a}_2 a_3 \mathrm{a}_4}{b_1 b_2 \, \mathrm{b}_3}$$

Following the above standards, the crack resistance safety factor K for high rockfill dam panels is generally taken between 1.3-2.2, with higher values preferable in cold regions. In this paper, 1.8 is adopted.

3 Project Case and Conditions

3.1 Project Overview

The Yangqu Hydropower Station project is located in Hainan Prefecture, Qinghai Province, situated on the inland plateau. The region experiences long, cold winters and short, cool summers. The average annual temperature is

2.3°C, with an extreme maximum temperature of 31.8°C and an extreme minimum temperature of -29.2°C. The coldest month has an average temperature of -11°C, categorizing it as a severely cold area. The average annual relative humidity is 54%. The dam crest elevation is 2721m, with a maximum dam height of 150m and a crest length of 354.67m. The upstream slope of the concrete face rockfill dam is 1:1.4, and the downstream slope, except for the first level at 1:1.4, is at 1:1.3. The dam body is divided into the upstream paving area, heavy cover area, bedding area, special bedding area, transition zone, upstream rockfill area, downstream rockfill area, bottom concrete dam, downstream revetment, and concrete face. The bedding area located below the panel serves as the support structure for the concrete face, designed with a horizontal width of 4m, and the slope ratio is the same as the bottom slope of the panel, arranged uniformly in width. The thickness of the concrete face varies, with the top being 0.3m thick and the bottom 0.56m, spanning construction elevations from 2631.0m to 2717.5m, a construction height of 86.5m, and the maximum panel length of 121.1m. The spacing between transverse joints is divided into 6m and 12m. The panel uses a single layer of bi-directional reinforcement, with a reinforcement ratio of 0.4% in each direction.

3.2 Computational Model

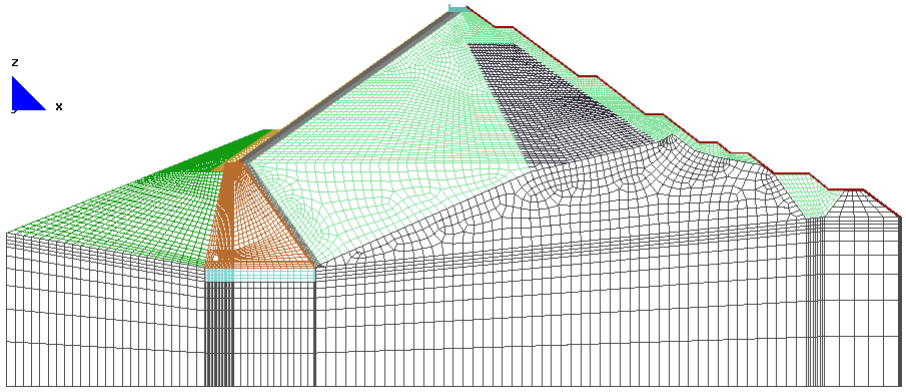

(a)

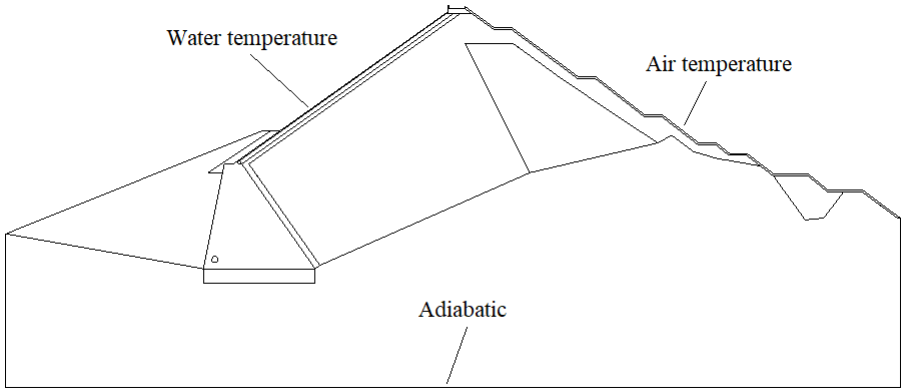

(b)

Figure 1. Grid model and boundary schematic

Considering the dam foundation, rockfill structure, bedding, and panel, a 12m single dam section panel model as shown in Figure 1 is established for the middle dam segment. The model comprises 127,344 elements and 141,947 nodes, primarily using 8-node hexahedral elements, with the reinforcement simulated using rod elements. The panel is divided into three layers along its thickness direction, with a no-thickness joint element set between the panel and the bedding. In terms of direction, x points towards the upstream-downstream direction, positive towards downstream; y points towards the left-right bank direction, positive towards the left bank; and z is vertical, positive upwards. The model foundation is fully constrained, with normal constraints on the sides. The model's bottom and side surfaces have adiabatic boundaries, the air contact part is a third-type heat dissipation boundary, and the part in contact with the reservoir water is a first-type heat dissipation boundary.

3.3 Calculation Conditions

The temperature conditions in the dam site area are shown in Table 2, and the main material parameters of concrete are shown in Tables 3-5.

The adiabatic temperature rise of concrete is assumed to be: $T = \frac{39.2t}{t+0.96}$;

The elastic modulus is taken as: $E(\tau) = 36.8\left(1 - e^{-0.32\tau^{0.9}}\right)$.

Table 2. Dam site area temperature conditions

Item	Month												Average
	Jan	Feb	Mar	Apr	May	Jun	Jul	Aug	Sep	Oct	Nov	Dec	(or Annual)
Average Temp. (°C)	-11	-7.0	-1	4.3	8.7	11.6	13.4	12.8	8.5	2.5	-4.9	-9.8	2.3
Extreme Max Temp. (°C)	134	139	20.6	27.7	26.6	27.9	31.8	29.2	289	26.7	17.0	11.1	31.8
Extreme Min Temp. (°C)	-29.2	-27.2	-21.6	-12.7	-6.3	-4.8	3.0	-1.2	-5.8	-14.2	-23.9	-26.5	-29.2

Table 3. Main material parameters of concrete

Specific Heat (kJ/(kg°C))	Thermal Diffusivity (10^{-3} m^2/h)	Thermal Conductivity (kJ/(mh°C))	Linear Expansion Coefficient (10^{-6}°C)	Density (g/cm^3)
0.900	3.8000	8.6600	8.400	2.45

Table 4. Autogenous volume deformation of concrete

Age (days)	0	1	2	3	5	7	10	14	21	28
Microstrain	0	-4.4	-8.5	-11.2	-15.9	18	-19.2	-19.8	-23.3	-26.2
Age (days)	35	40	50	60	70	80	90	105	120	
Microstrain	-29	-31	-32	-34	-35.2	-37	-37.8	-39.8	-42.2	

Table 5. Concrete strength

Type	Strength (MPa)		
	7 days	28 days	90 days
Compressive Strength	26	39	45
Split Tensile Strength	1.9	2.6	3.1
Axial Tensile Strength	2.2	3.2	3.8
Allowable Strength (Crack Resistance Coefficient 1.8)	1.22	1.78	2.11

3.4 Analysis Conditions

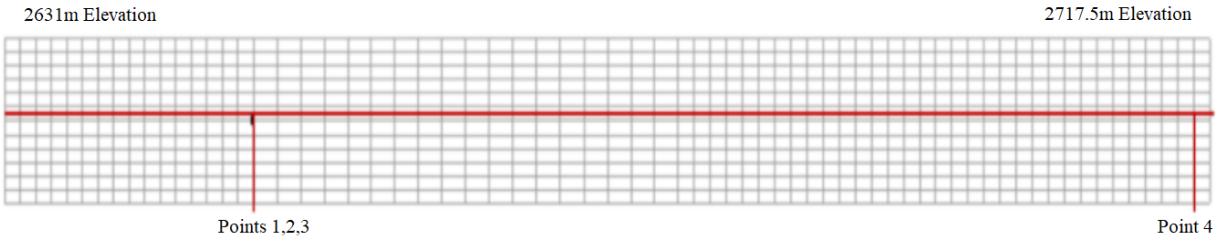

Figure 2. Distribution of panel characteristic points

The factors affecting panel stress involve loads, constraints, and performance parameters, where construction period loads mainly include self-weight load, temperature load (ambient temperature, cold snap, daily temperature difference), shrinkage load, and rockfill body deformation load; constraints mainly include bedding constraints and reinforcement constraints; performance parameters include concrete casting temperature, adiabatic temperature rise,

and autogenous volume deformation. Among these factors, the impact of panel self-weight load is small and is not analyzed.

For ease of stress analysis, points 1 to 3 located at the elevation of 2650m along the thickness direction of the panel from the surface inward are taken as characteristic points, as shown in Figure 2.

4 Construction Period Load Impact Analysis

4.1 Temperature Impact

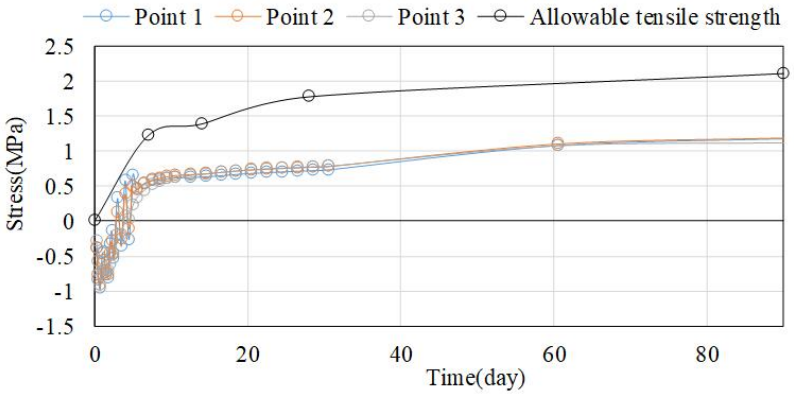

Figure 3. Relationship between stress and strength of panel characteristic points cast in July

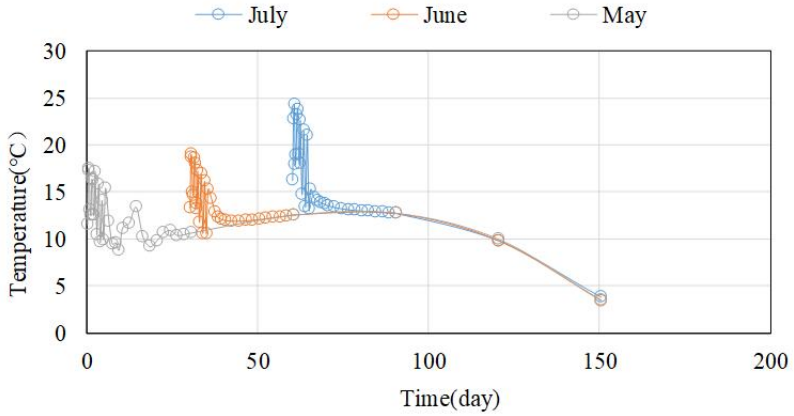

Figure 4. Temperature change of panel surface cast in different months

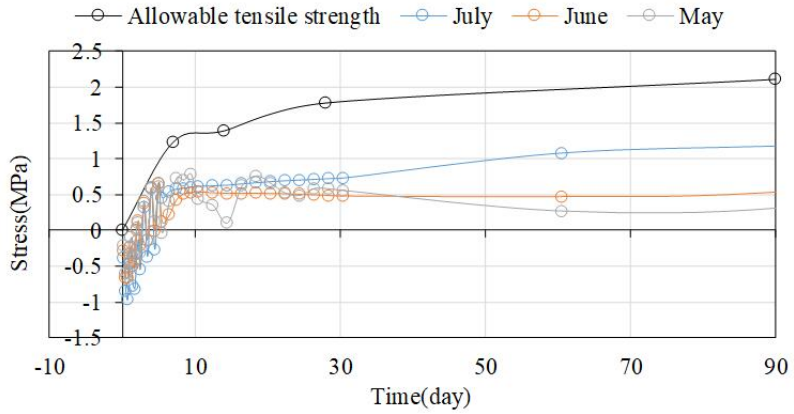

Figure 5. Relationship between slope-direction stress and strength of panel surface points cast in different months

Based on actual project conditions, the panel construction is set between May and July, with average temperatures of 8.7°C, 11.6°C, and 13.4°C, respectively. With the casting temperature set at 10°C, without considering insulation and under normal environmental temperature load, the stress change at the characteristic points of the panel cast in July and its relationship with allowable strength are shown in Figure 3. The surface point temperature changes, stress changes, and their relationship with allowable strength for the three months are presented in Figures 4 and 5.

The analysis indicates that when casting in July, the panel temperature rapidly rises after concrete casting due to hydration, reaching the highest temperature around 1.5∼2 days, then gradually decreases, dropping to the average temperature around 10 days; the highest surface temperature of the panel is about 26.7°C, gradually decreasing towards the bottom, with the highest bottom temperature about 21.7°C. The development of stress shows that in the early stages, as the temperature rises and the panel expands, it is generally in a state of compression; as the temperature decreases, the panel overall contracts, but the surface contracts faster than the inside, and the top contracts faster than the bottom, turning into a state of tension around 3 days. As the temperature further decreases, the panel is generally in a state of tension. The slope-direction stress is highest in the middle and lower parts of the panel along the elevation, gradually decreasing towards the top and bottom. The calculated slope-direction stress is less than the corresponding age strength of concrete, but the crack resistance safety factor is generally close to 1.8 within 10 days, indicating a small safety margin. As the environmental temperature decreases, the highest temperature of the panel decreases, reducing the maximum slope-direction stress slightly, but the reduction is not significant, and the early age crack resistance safety factor remains close to 1.8.

Apart from normal environmental temperatures, daily temperature differences cause varying panel stresses. With significant daily temperature differences in the Qinghai area and considering differences of 25°C, 22°C, 19°C, the maximum tensile stress on the concrete panel surface at 5 days age reaches 1.10MPa, 0.93MPa, 0.92MPa respectively, as shown in Figure 6, but the high tensile stress is limited to the surface, decreasing to below 0.5MPa just 0.12m below the surface. This stress value is related to the mesh size but clearly shows the significant impact of daily temperature differences on surface stress.

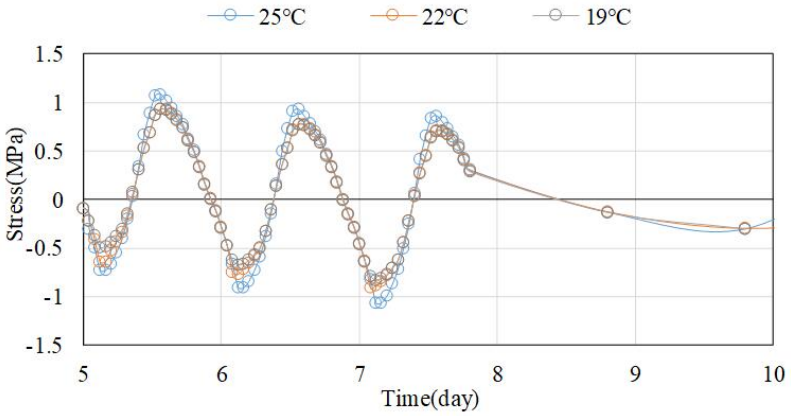

Figure 6. Comparison of slope-direction stress changes under different daily temperature differences

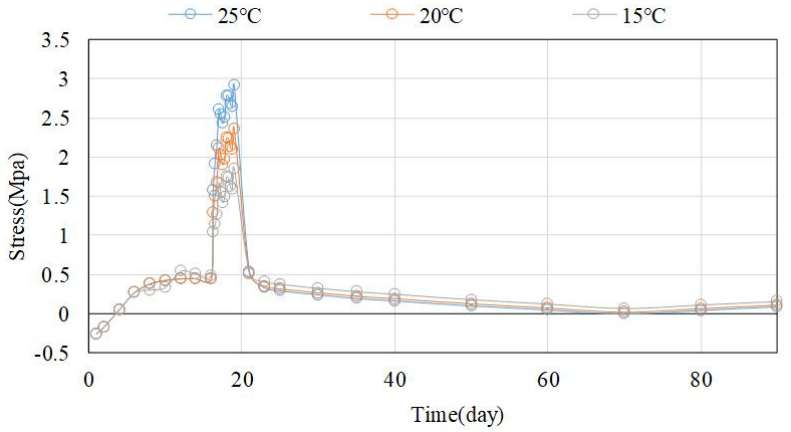

Figure 7. Comparison of slope-direction stress changes under different cold wave impacts

The standard for cold waves in northern China is a temperature drop of more than 10°C in 24 hours or more than 12°C in 48 hours, with the lowest temperature below 4°C. In the analysis, considering a temperature drop of 25°C, 20°C, 15°C over three days at 15 days age, the maximum tensile stress on the panel surface in the slope direction is 2.6MPa, 2.1MPa, 1.67MPa respectively, with increases of 2.1MPa, 1.6MPa, 1.17MPa, as shown in Figure 7. An increase of 1°C in temperature drop leads to an increase of about 0.1MPa in tensile stress; considering only the cold wave factor, 15 days age concrete can withstand a temperature drop of about 10°C.

4.2 Shrinkage Impact

Considering a concrete permeability coefficient of 2×10^{-8} m/d, environmental humidity of 40%, and a shrinkage coefficient of 1.5×10^{-3}, when humidity changes between 0.6∼1.0, the shrinkage strain increment is directly proportional to the humidity increment. The analysis indicates that early concrete shrinkage primarily occurs on the surface, forming internal and external moisture differences and a shrinkage deformation gradient, progressively developing inward; shrinkage stress increment is mainly concentrated in the early age, reaching about 1.55MPa at 30 days, then gradually stabilizes, with the tensile stress mostly limited within 5cm of the surface. If panel moisturizing measures are inadequate, shrinkage stress may lead to panel cracking.

4.3 Impact of Rockfill Body Deformation

The rockfill body undergoes deformation during both the construction period and the water storage period, with overall settlement deformation occurring before water storage, and overall bending deformation of the panel occurring after water storage. This analysis mainly considers the deflection deformation of the panel after water storage. According to monitoring data, the deformation values at the upper and lower ends of the Nazixia panel are small, with significant deformation occurring in the middle section. The deformation pattern is shown in Figure 8, with the maximum deflection approximately 14cm. The height of this project is similar to that of Nazixia, and calculations are based on the deflection deformation observed in Nazixia. The analysis indicates that under this deflection deformation condition, the concrete panel is primarily subjected to an increase in compressive stress, with the maximum increase in slope-direction tensile stress being 0.3MPa, and the maximum increase in compressive stress being 0.9MPa, as shown in Figure 9. Thus, bending deformation during the water storage period does not result in significant tensile stress on the panel surface, contributing little to cracking. The direction of bending deformation of the rockfill body before water storage may be opposite to that caused by water storage pressure, which could put the panel under tension. However, due to data limitations, this paper does not provide a quantitative analysis.

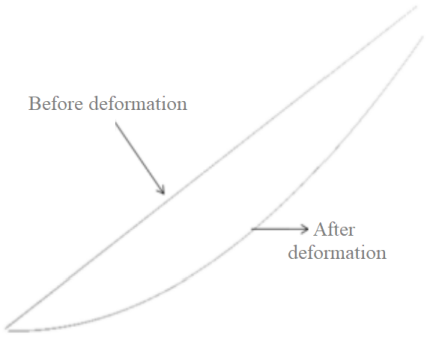

Figure 8. Schematic of rockfill body deflection deformation

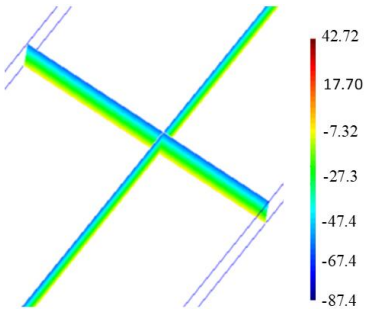

Figure 9. Stress cloud diagram in slope direction under post-water storage bending deformation conditions (0.01MPa)

5 Impact of Constraints and Performance Parameters

5.1 Reinforcement Constraint

Panel reinforcement affects the panel's stiffness and stress state. Below the elevation of 2650m, longitudinal rebars Φ28@20 and transverse rebars Φ25@20 are laid, while above 2650m, both longitudinal and transverse rebars are Φ25@20, simulated as rod elements. The analysis indicates that adding dense reinforcement significantly increases the structural stiffness, resulting in an increase in structural stress of about 0.4MPa under the same temperature changes and autogenous volume deformation of concrete. The stress distribution pattern of the panel with and without reinforcement shows slight differences, with a larger stress increment in the middle region after reinforcement, and a slightly smaller increment at the edges (as shown in Figure 10). Increasing reinforcement mainly serves to limit cracking, having a minimal effect on improving panel crack resistance.

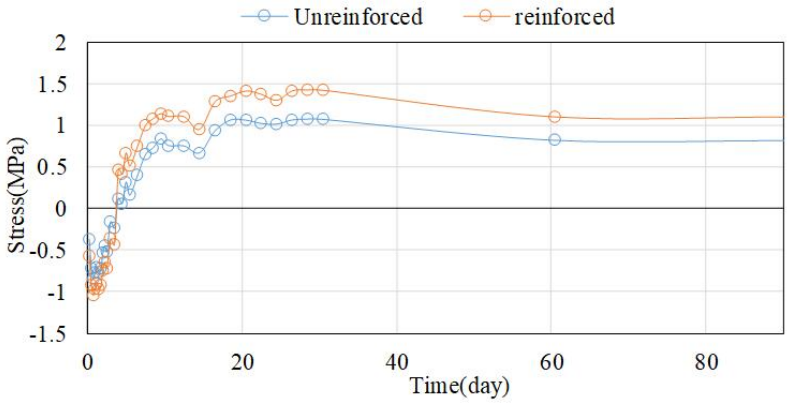

Figure 10. Comparison of slope-direction stress changes under different reinforcement scenarios

5.2 Bedding Constraint

The panel deformation is affected by the degree of constraint from the bedding, with greater constraints resulting in higher stress under temperature loads, etc. Friction coefficients are used to consider different constraints between the bedding and the panel, showing that while the overall degree of constraint varies, the overall stress distribution and variation pattern are similar, but with different stress values. The friction coefficient value is taken based on the literature [30] and combined with the actual engineering.With a friction coefficient of 0.7, the maximum slope-direction stress is 1.10MPa, and with 0.5, it is 0.95MPa, a 14% reduction, as shown in Figure 11, indicating that reducing the degree of constraint between the panel and bedding effectively improves the panel's stress state.

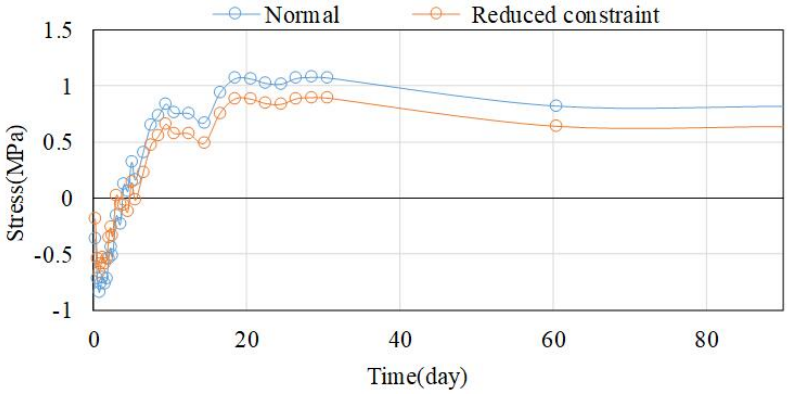

Figure 11. Comparison of slope-direction stress changes under different constraint conditions

5.3 Casting Temperature Impact

Considering panel casting in May with casting temperatures of 10°C, 8°C, and 6°C, the highest temperatures are 21.5°C, 20.4°C, and 19.3°C, respectively, as shown in Figure 12, A 2°C increase in casting temperature results in approximately a 1°C increase in the highest temperature; the higher the maximum temperature, the greater the stress, with maximum slope-direction stresses of 0.88Mpa, 0.78Mpa, and 0.67Mpa, respectively, as shown in Figure 13. A

1°C difference in maximum temperature corresponds to a difference of about 0.05∼0.085MPa in maximum stress. Considering the concrete's allowable tensile strength, the minimum crack resistance safety factor between 4-7 days is smallest, with corresponding minimum safety factors of 2.60, 2.17, and 1.83 for the three scenarios.

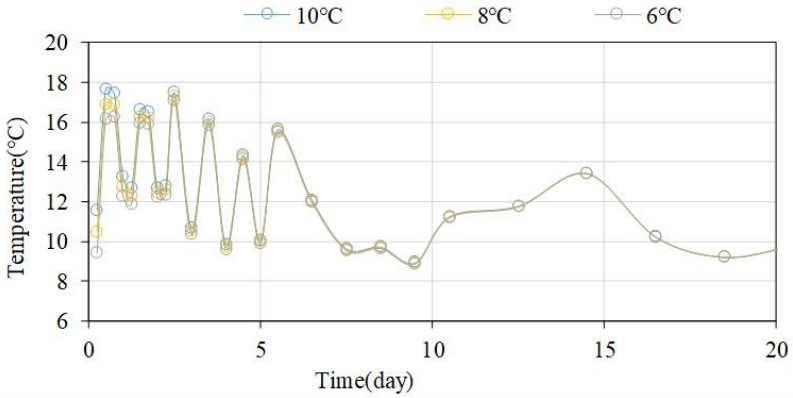

Figure 12. Comparison of panel temperature changes under different casting temperatures

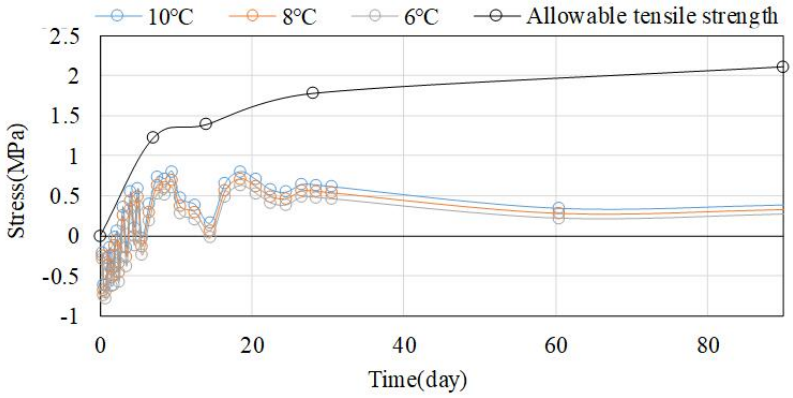

Figure 13. Comparison of slope-direction stress changes under different casting temperatures

5.4 Adiabatic Temperature Rise Impact

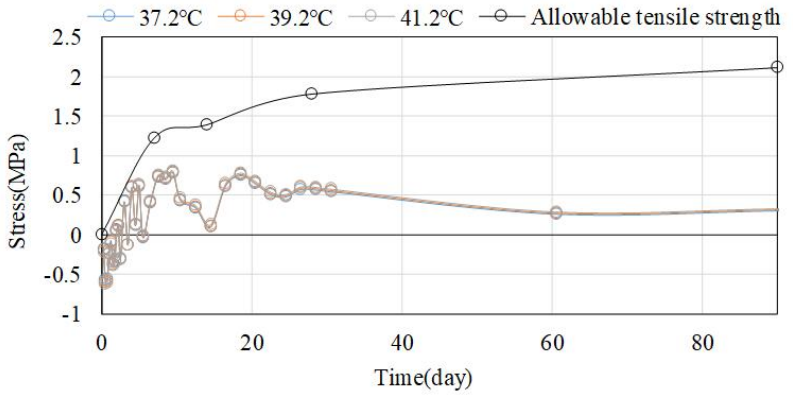

Figure 14. Comparison of slope-direction stress changes under different adiabatic temperature rises

The adiabatic temperature rise affects the development of concrete temperature. Considering final adiabatic temperature rises of 37.2°C, 39.2°C, 41.2°C, with other conditions being the same, each 1°C increase in the maximum value of adiabatic temperature rise raises the maximum panel temperature by 0.275°C, with a corresponding increase in maximum tensile stress of 0.005∼0.01MPa, a minor change, as shown in Figure 14. The minimum crack resistance

safety factors under the three scenarios are 1.86, 1.83, and 1.80, respectively, indicating that a variation within 5°C in adiabatic temperature rise has an insignificant impact on panel crack resistance.

5.5 Autogenous Volume Deformation Impact

Concrete's autogenous volume deformation mainly occurs in the early age, with shrinkage deformation inducing an increase in tensile stress and expansion deformation causing an increase in compressive stress. Considering shrinkage, no deformation, and slight expansion deformation scenarios, the maximum slope-direction stresses are 0.88Mpa, 0.66MPa, and 0.61MPa, respectively, with the minimum crack resistance safety factors between 4-7 days being 1.83, 2.3, and 2.4, as shown in Figure 15. Thus, concrete with a slight expansion agent significantly reduces panel tensile stress and improves crack resistance.

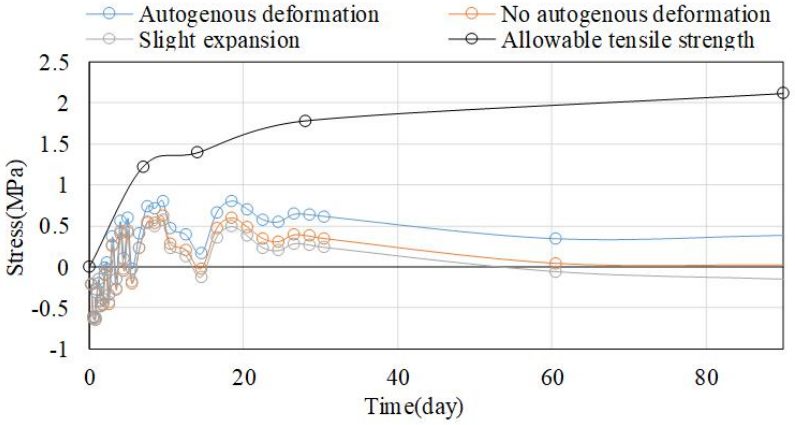

Figure 15. Comparison of slope-direction stress changes under different autogenous volume deformations

5.6 Impact of Linear Expansion Coefficient

The size of the linear expansion coefficient, affected by different raw materials such as concrete aggregates, in turn influences temperature stress. Considering different linear expansion coefficients, set at 8.4×10^{-6} and 7.4×10^{-6}, the maximum slope-direction stresses are respectively 0.88MPa and 0.77MPa, as shown in Figure 16. The minimum crack resistance safety factors between days 4 to 7 for these two scenarios are respectively 1.83 and 2.20. Using concrete with a smaller linear expansion coefficient is more effective for crack prevention in the panel.

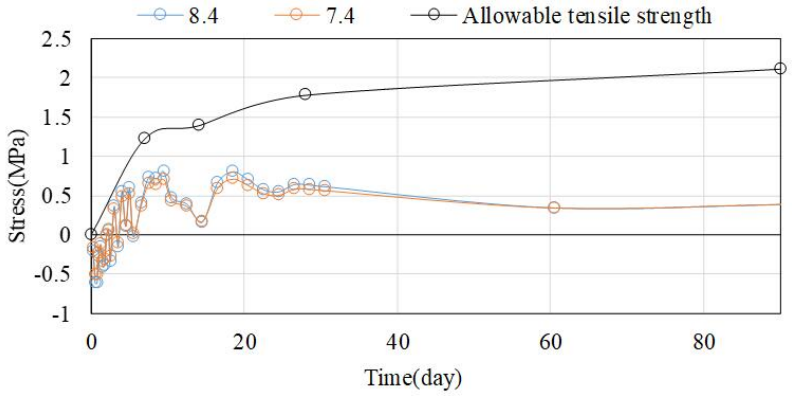

Figure 16. Comparison of slope-direction stress changes under different linear expansion coefficients ($\times 10^{-6}$/°C)

6 Research Conclusions

This paper briefly summarizes the main factors influencing panel cracking in cold regions and, using the Yangqu panel rockfill dam project as a case study, conducted a simulation analysis on panel stress and crack resistance capabilities, yielding the following conclusions:

(1) Regarding loads, environmental temperature in cold regions is the dominant factor causing stress exceedance and cracking, with daily temperature differences and cold snaps acting as inducing factors. Shrinkage is mainly concentrated on the surface and has minimal impact under good water curing conditions. Initial water storage

bending deformation does not significantly increase surface tensile stress on the panel, contributing little to cracking. However, deformation of the bedding towards the upstream during the construction period may cause a significant increase in tensile stress.

(2) Concerning constraints, reinforcement increases structural stiffness, leading to an increase in structural stress under the same temperature changes and autogenous volume deformation, having a minimal impact on temperature control and crack prevention. The less the bedding constrains the panel, the lower the stress produced in the concrete panel, and reducing the constraint between the panel and bedding can improve the stress state of the panel.

(3) In terms of performance parameters, higher casting temperatures result in lower crack resistance safety factors, with a significant impact. An increase in concrete's adiabatic temperature rise increases the panel's tensile stress, but the amount of increase is limited. Within a certain range, variations do not significantly affect the panel's crack resistance performance. Both autogenous volume deformation and linear expansion coefficient significantly affect stress, with the degree of impact directly related to the magnitude of the parameters.

(4) The crack resistance safety factor for rockfill dam panels can refer to the concrete crack resistance safety factor given for concrete dams, and values can be taken within the range of 1.3-2.2. For high dam panels in cold regions, higher values may be used.

(5) Based on the results of computational analysis, the casting temperature of panel concrete in cold regions and the corresponding maximum temperature must be strictly controlled. Insulation measures should effectively mitigate the effects of daily temperature differences and potential cold snaps. The necessity for dense reinforcement is minimal, and where possible, concrete types with low shrinkage or slight expansion should be used.

Funding

This work was supported by the National Key Research and Development Program of China (Grant No.: 2021YFC3090100).

Data Availability

The data used to support the findings of this study are available from the corresponding author upon request.

Conflicts of Interest

The authors declare that they have no conflicts of interest.

References

[1] X. D. Lv and J. Z. Li, "Cracks in face slab of concrete-faced rockfill dam: Present situation, causes of formation, and progress of prevention technologies," *J. Yangtze River Sci. Res. Inst.*, vol. 38, no. 11, pp. 127–134,141, 2021. https://doi.org/10.11988/ckyyb.20210378

[2] Y. Arici, "Investigation of the cracking of CFRD face plates," *Comput. Geotech.*, no. 38, pp. 905–916, 2011. https://doi.org/10.1016/j.compgeo.2011.06.004

[3] X. F. He, Z. L. Wang, and Q. He, "Cause analysis of face cracking of a CFRD during construction period in cold regions," *Adv. Sci. Technol. Water Resour.*, vol. 39, no. 3, pp. 68–74, 2019. https://doi.org/10.3880/j.issn .1006-7647.2019.03.012

[4] Y. Arici, "Behaviour of the reinforced concrete face slabs of concrete faced rockfill dams during impounding," *Struct. Infrastruct. Eng.*, no. 9, pp. 877–890, 2013. https://doi.org/10.1080/15732479.2011.631111

[5] Z. P. Xu, "Research progresses and key technologies of CFRD construction," *J. Hydraul. Eng.*, vol. 50, no. 1, pp. 62–74, 2019.

[6] P. Marques Filho and N. L. S. De Pinto, "CFRD dam characteristics learned from experience," *Int. J. Hydropower Dams*, vol. 12, no. 1, pp. 72–76, 2005.

[7] M. Yuan, S. Qiang, W. J. Cen, Y. Hu, and B. Chen, "Causes and prevention of cracks in concrete slab of rockfill dam during construction," *J. Basic Sci. Eng.*, vol. 31, no. 4, pp. 811–827, 2023.

[8] J. Z. Li, "Causes of cracking on long concrete face plate of rockfill dam manufactured by one-off construction technique in cold region," *J. Yangtze River Sci. Res. Inst.*, vol. 37, no. 8, pp. 1–8, 2020. https://doi.org/10.119 88/ckyyb.20200049

[9] Z. F. Zhao, Z. H. Zheng, S. W. Ji, Z. G. Zhao, and T. Shi, "Simulation of temperature and stress fields in concrete face slabs of rockfill dams," *J. Zhejiang Univ. Technol.*, vol. 51, no. 2, pp. 119–126, 2023. https://doi.org/10.3969/j.issn.1006-4303.2023.02.001

[10] H. Chen, G. Deng, Y. Zhang, and Y. Q. Zhang, "Simulation of faced rockfill dams considering temperature change and long-term deformation," *J. Hydroelectric Eng.*, vol. 40, no. 10, pp. 124–134, 2021. https://doi.org/ 10.11660/slfdxb.20211012

[11] Z. F. Zhao, X. Wu, Z. Y. Zhang, J. Y. Qi, G. B. Zhang, and J. M. Xu, "Thermal expansion coefficient of carbon nanotubes reinforced face slab concrete of rockfill dam at early age," *Bull. Chin. Ceram. Soc.*, vol. 40, no. 2, pp. 465–472, 512, 2021.

[12] Z. Q. Xie, Z. J. Zhang, Y. Dong, and C. Wu, "Numerical simulation-based study of method for temperature control and crack prevention of concrete face slab of rock-fil dam during construction," *Water Resour. Hydropower Eng.*, vol. 49, no. suppl. 1, pp. 33–41, 2018.

[13] Z. L. Zhang, B. Y. Zhang, M. Z. Zhou, W. J. Yin, and Y. L. Feng, "Numerical analysis of thermal stress induced by solar radiation in concrete-faced rockfill dams," *Chin. J. Geotech. Eng.*, vol. 43, no. 11, pp. 1957–1966, 2021. https://doi.org/10.11779/CJGE202111001

[14] K. M. Wei, H. Zhou, Z. K. Mi, G. Y. Li, and Z. Deng, "Reinforcement calculation of concrete slab in concrete faced rockfill dams," *Chin. J. Geotech. Eng.*, vol. 45, no. 06, pp. 1314–1322, 2023. https://doi.org/10.11779/CJGE20220757

[15] C. Yang, F. N. Dang, H. B. Xue, and J. Gao, "Mechanism of structural tensile damage to concrete face slabs of high CFRDs in narrow valley regions and improvements," *J. Hydroelectric Eng.*, vol. 36, no. 04, pp. 95–103, 2017. https://doi.org/10.11660/slfdxb.20170411

[16] Y. T. Liu, D. J. Zheng, X. Wu, and E. H. Cao, "Numerical analysis of cracks in underwater face slab of concrete face rockfill dam," *J. Yangtze River Sci. Res. Inst.*, vol. 38, no. 12, pp. 152–157, 2021. https://doi.org/10.11988/ckyyb.20200799

[17] R. P. Li, J. W. Xu, X. Y. Liu, H. Y. Mao, and L. J. Wang, "Impact analysis of convex terrain on stress-strain and deformation characteristics of CRFD," *J. Hohai Univ. (Nat. Sci.)*, vol. 51, no. 06, pp. 53–60, 2023. https://doi.org/10.3876/j.issn.1000-1980.2023.06.007

[18] Z. M. Jiang, J. Y. Yang, P. Sun, and J. H. Liao, "Rheological characteristics and face slab's disengagement of Sanbanxi concrete face rockfill dam," *J. Yangtze River Sci. Res. Inst.*, vol. 39, no. 06, pp. 120–126+137, 2022. https://doi.org/10.11988/ckyyb.20210244

[19] X. J. Kong, Y. Q. Qu, D. G. Zou, K. Zeng, and J. M. Liu, "Cross-scale crack evolution analysis for face slab in concrete faced rockfill dams under strong earthquake," *Chin. J. Geotech. Eng.*, vol. 42, no. 06, pp. 989–996, 2020. https://doi.org/10.11779/CJGE202006001

[20] M. Saberi, C. D. Annan, and J. M. Konrad, "Seismic response analysis of face slabs in concrete face rockfill dams," *J. Earthquake Eng.*, vol. 26, no. 1, pp. 192–220, 2022. https://doi.org/10.1080/13632469.2019.1666756

[21] H. Zhou, J. Liu, and X. Lu, "Safety demonstration of compound structure extra-high face rockfill dam," *Water Resour. Power*, vol. 40, no. 3, pp. 87–90, 2022.

[22] Z. J. Wang, S. H. Liu, L. J. Li, and L. J. Wang, "Numerical analysis of the causes of slab's cracks on Gongboxia face rockfill dam," *J. Hydraul. Eng.*, vol. 45, no. 3, pp. 343–350, 2014.

[23] M. Zhang, Z. X. Zheng, and G. F. Lv, "Characteristics and cause analysis of cracks on face slabs of Gongboxia CFRD," *J. Zhejiang Water Conserv. Hydropower Coll.*, vol. 32, no. 3, pp. 30–33, 2020. https://doi.org/10.3969/j.issn.2095-7092.2020.03.007

[24] *Code for the Design of Hydraulic Concrete Structures: BN/T 11011-2022*. Beijing: China Water & Power Press, 2022.

[25] *Code for Design of Concrete face Rockfill Dam: NB/T10871-2021*. Beijing: China Water & Power Press, 2021.

[26] B. F. Zhu, *Thermal Stresses and Temperature Control of Mass Concrete*. New York: Elsevier, 2014.

[27] G. X. Zhang, "Development and application of SAPTIS-A software of multi-field simulation and nonlinear analysis of complex structures (Part I)," *Water Resour. Hydropower Eng.*, vol. 44, no. 1, pp. 31–44, 2013. https://doi.org/10.3969/j.issn.1000-0860.2013.01.008

[28] Y. Z. Liu, G. X. Zhang, P. Yang, and S. W. Zhou, "Key technical issues and optimization analysis on temperature control and crack prevention measures for Xiluodu super-high arch dam during the construction period," *Appl. Mech. Mater.*, vol. 584–586, pp. 2043–2051, 2014. https://doi.org/10.4028/www.scientific.net/amm.584-586.2043

[29] B. F. Zhu, "On coefficients of safety for crack prevention of concrete dams," *Water Resour. Hydropower Eng.*, no. 07, pp. 33–37, 2005. https://doi.org/10.3969/j.issn.1000-0860.2005.07.010

[30] L. F. Wen, Y. L. Li, and J. R. Chai, "Numerical analysis of plastic damage of concrete cutoff wall for concrete face rockfill dam," *J. Hydraul. Eng.*, vol. 52, no. 6, pp. 673–688, 2021.